We are IntechOpen, the world's leading publisher of Open Access books Built by scientists, for scientists

6,900
Open access books available

185,000
International authors and editors

200M
Downloads

Our authors are among the

154
Countries delivered to

TOP 1%
most cited scientists

12.2%
Contributors from top 500 universities

WEB OF SCIENCE™

Selection of our books indexed in the Book Citation Index in Web of Science™ Core Collection (BKCI)

Interested in publishing with us?
Contact book.department@intechopen.com

Numbers displayed above are based on latest data collected.
For more information visit www.intechopen.com

12

Novel Conductive and Transparent Optical Fiber Probe for Multifunctional Scanning Tunneling Microscopy

Guo Xinli[1,2] and Fujita Daisuki[3]
[1]*School of Materials Science & Engineering, Southeast University, Nanjing, Jiangsu,*
[2]*Jiangsu Key Laboratory for design and Manufacture of Micro-Nano Biomedical Instruments*
[3]*Advanced Nanocharacterization Center, National Institute for Materials Science, Tsukuba, Ibaraki,*
[1,2]*P. R. China*
[3]*Japan*

1. Introduction

It is well known that progress in modern science is impossible without reliable tools for characterization of structural, physical, and chemical properties of materials and devices at the micro-, nano, and atomic scale levels. The structural information of materials can be obtained by the 1st generation of optical microscopy, and second generation of scanning and transmission electron microscopy. While characterization of local electronic properties became possible after the 3rd generation of Scanning Tunneling Microscopy (STM) based on the quantum mechanical tunneling between an atomically sharp metallic tip and conductive surface by G. Binning and H. Rohrer in 1981 at IBM Zurich, which earned the Nobel Prize in Physics five year later [Binning et al, 1982, 1983]. STM has become the first instrument to directly probe local geometries of various nanostructures with an atomic resolution and has triggered development of new classes of STM-related techniques and a rapid growth of a variety of scanning probe microscopy (SPM) techniques over the last two decades, which include atomic force microscopy (AFM) based on the mechanical detection of the Van der Waals forces between the tip and the sample surface using a pliable cantilever[Binning et al, 1986, magnetic force microscopy (MFM), electrostatic force microscopy (EFM), scanning capacitance microscopy (SCM), near-field scanning optical microscopy (NSOM) etc to provide capability to access local electrical, magnetic, chemical, mechanical, optical, and thermal properties of materials on the nanometer scale. The SPM technique has demonstrated not only imaging, but also manipulation, control and modification of the local structure and material functionality at the nano-and atomic level. The rapid development of nanoscience and nanotechnology was really started and strongly stimulated by the generation and availability of SPM techniques, and in turn constantly stimulates development of novel SPM techniques [Sergei & Alexei, 2007]. Typically, one of the advancement of STM under the stimulation of nanometer-scale science and technology is to detect and analyze not only tunneling electrons but also photons induced by tunneling

electrons [Berndt, 1998]. This kind of STM-induced photon emission, or STM-induced luminescence (STML) is a local energy-dissipation process where a part of the energy carried by a tunneling electron is transferred to a radiative process, it has the potential ability to unveil local electronic structures and chemical states with high spatial resolution up to atomic scale, and the fabrication of nanoscale light source. Up to date, STML has been successfully observed on various surface nanostructures including metal surfaces [Berndt et al, 1993a, 1995; Uehara et al, 1999], indirect-gap semiconductor surfaces [Downes & Welland, 1998; Thirstrup et al, 1999], direct-gap semiconductors [Sasaki & Murashita, 1999; Fujita et al, 2004; Guo et al, 2007], fluorescence molecules [Berndt et al, 1993b; Fujita et al, 2001; Dong et al, 2004; Guo et al, 2003, 2004], conjugated polymer films [Alvarado et al, 1997 & Lidzey et al, 1997], quantum nanostructures [Evoy et al, 1999 & Tsuruoka et al, 2003] etc.
The STML is believed to be realized by the excitation of highly localized tunneling current of a STM through following two ways as schematically shown in figures 1 (a) and (b).

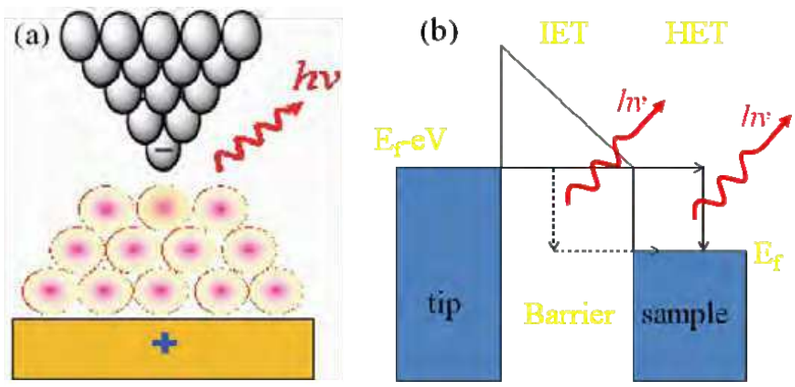

Fig. 1. Schematic drawing of the STML from molecular surface in STM tunneling junction (a), and (b) band gap in STM tunneling junction to show the two types of excitation process of STML. i.e: Inelastic Electron Tunneling (IET), and Hot Electron Thermalization (HET).

The inelastic tunneling (IET) process in figure 1 (b) shows that photon emission is triggered by an inelastic process during electron tunneling through the barrier. The STML process from metal and indirect band-gap semiconductor surfaces can be well explained by the IET process i.e.: the tunneling electrons excite a localized surface plasmon or a tip-induced plasmon (TIP) whose radiative decay processes cause light emission (Downes et al., 1998; Johansson, 1998, 1990). While the "hotelectron thermalization (HET)"process in figure 1(b) shows that energetic electrons injected into the sub-surface layers lose their energy in the bulk by a so-called "thermalization" process, and finally recombine with positive holes that emit photons. The STML process from the direct bandgap semiconductors and their quantum nanostructures can be well explained by the HET process i.e.: a part of tunneling electrons injected from an STM tip combine with major carriers (positive holes) to form excitons at low temperatures, which subsequently decay radiatively or non-radiatively. In addition, the electron-hole recombination process is also a reasonable explanation for the STML of organic semiconductor thin films (Alvarado et al., 1997; Lidzey et al., 1997), which has been studied with relation to the industrial applications for organic thin-film lightemitting devices (Friend et al., 1999; Lidzey et al., 1998).
There are two types of photon detection system for STML measurements as show in figures 2(a) and (b).

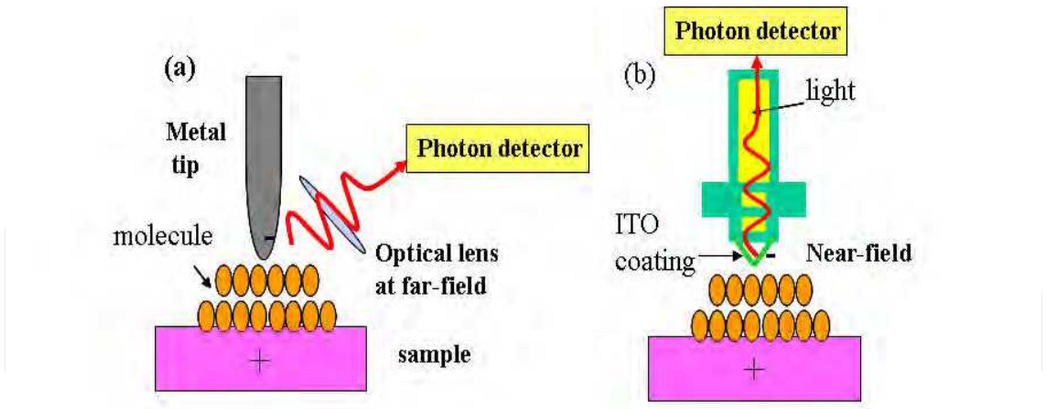

Fig. 2. Schematic drawing of the two types of photon detection systems for STML measurements: (a) optical far-field photon detection by setting optical lens of fibers near to the STM tunneling junction; (b) optical near-field photon detection by using a conductive and transparent optical fiber probe.

In Figure 2(a), the emitted photons in STML measurements are normally collected at optical far-field using lenses (Dong et al., 2002; Hoffmann et al., 2002), fibers (Arafune et al., 2001; Thirstrup et al., 1999), or ellipsoidal reflectors (Nishitani et al., 1998; Suzuki et al., 1999) to focus light from a tip to a detector outside. This system have been widely used due to its relatively easy instrumentation (Arafune et al., 2001; Dong et al., 2002; Hoffmann et al., 2001, 2002; Nazin et al., 2003; Nishitani et al., 1998; Suzuki et al., 1999; Thirstrup et al., 1999). The other detection system is shown in figure 2 that the emitted photons are collected within the optical near-field into a conductive and transparent optical fiber probe. This system is first developed by Murashita (1999), which has a great similarity with near-field scanning optical microscopy (NSOM) operating in collection mode, where an optical fiber probe is used for collection of light (Garcia-Parajo et al., 1994). This near-field photon detection offers a unique capability of near-field detection and potential high detection efficiency.
In this chapter, we introduce the application of a Novel Conductive and Transparent optical fiber probe for multifunctional scanning tunneling microscropy. This kind of novel probe have the functions for high-quality scanning tunneling microscope (STM) imaging, near-field excitation and detection of high-intensity STM-induced electroluminescence (STML). The probe is fabricated by coated a sharpened an optical fiber with an uniform ITO layer with the thickness in the range of ~50 nm to ensure the conductivity and improve the tip-apex geometry of the fiber probe High-quality STM image, and high-intensity STML corresponding to a maximum quantum efficiency of 7×10^{-4} and 1×10^{-3} photons/electron was obtained respectively on Au(111)/mica and p-GaAs(110) surface at room temperature (RT) by using of this fiber probe. This kind of novel conductive and transparent optical fiber probe provided a new way for equipping the STM not only with the functions of conventional STM but also with the functions of near-field excitation and detection of high-intensity STML.

2. Experimental procedure

2.1 Novel optical fiber probes for STML

Figures 3(a) and (b) show the SEM images of a novel optical fiber probe used for photon detection and STM imaging.

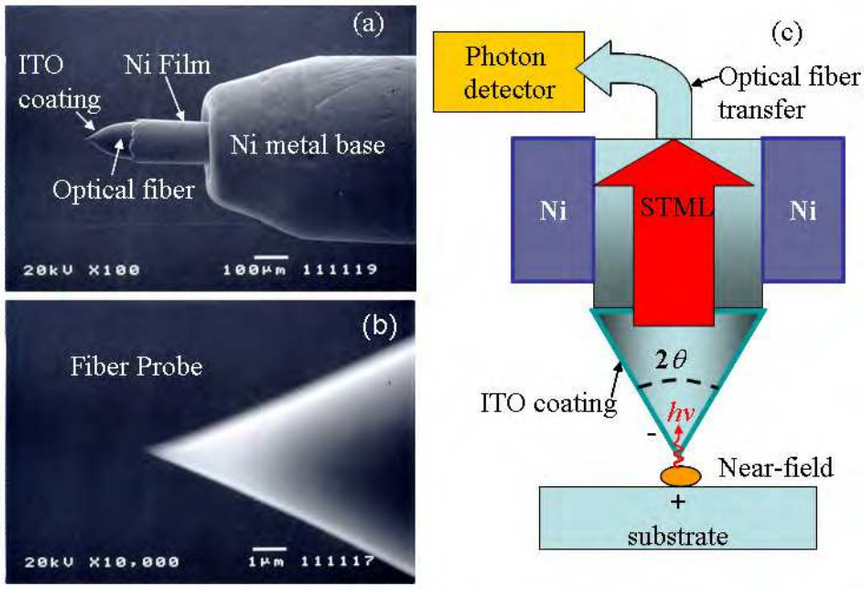

Fig. 3. (a)-(b): SEM images of a conductive and transparent STM fiber probe taken at different magnifications. The fiber probe is coated with 100-nm-thick indium-tin-oxide (ITO) thin film. (c): Schematic drawing of the optical near-field detection geometry for STML using the conductive and transparent fiber probe and its light transfer.

The optically transparent STM probes consisting of a GeO_2-doped multimode silica optical fiber with a core diameter of 100 µm and a sharpened tip apex are fabricated by NTT-AT Ltd., Japan. The a conductive indium-tin oxide (ITO) film is famous for its good electrical conductivity and optical transparency in the wide wavelength regions ranging from ultraviolet (UV), visible, to near infrared (NIR). The apex of the probe is coated with a conductive indium-tin oxide (ITO) thin film of 100-nm thickness with an optical transmission ~75%. Typical curvature of the tip apex of the optical fiber probe is 50–100 nm. As shown in Figure 3(c), photons emitted just under the probe apex are collected at near-field into the core of the optical fiber probe and transferred to the detectors outside. The cone solid angle with apex angle of 2θ is the area of a spherical cap on an unit sphere: $\Omega = 2\pi(1-\cos\theta) \sim 0.842$ [sr]. In addition,

2.2 STM equipped with photon detection system for STML

The STML is realized by the combination of a STM system with a photon detection system as schematically shown in Figure 4.

For the STM system in Figure 4, we use an ultrahigh vacuum system (UHV) with a base pressure ~3×10^{-9} Pa, which consists of a low temperature (LT)-STM chamber, a sample preparation chamber, and a deposition chamber. The whole LT- STM system manufactured by Unisoku Ltd., Japan, is installed on an air-dumping system. The STM head is suspended under a liquid helium/nitrogen cryostat with an internal eddy-current damping system. The sample can be cooled down to about 10 K by liquid helium in a tank through a bundle of copper wires for thermal connection. The lowest temperature of 8.7 K at the STM head has been achieved by pumping liquid helium in the tank. This practical UHV-LT-STM is shown in figure 5.

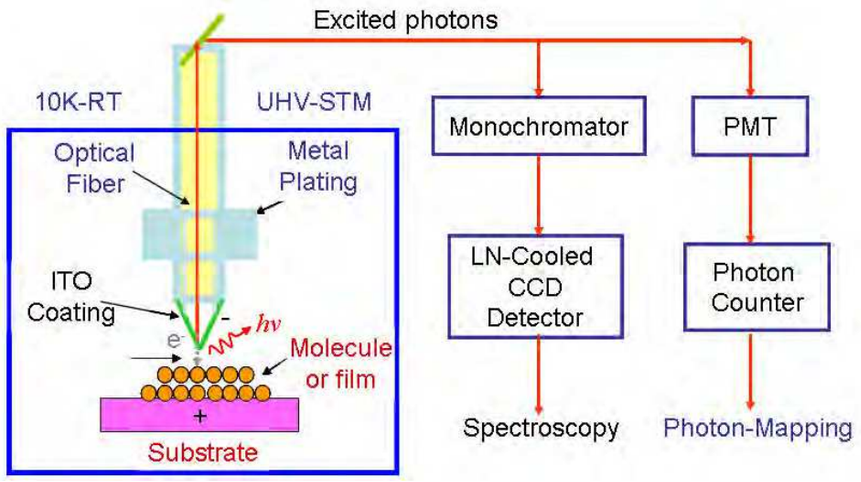

Fig. 4. Schematic drawing of the experimental set up for STML detection using an ITO-coated optical fiber probe based on the combination of a STM system with a photon detection system.

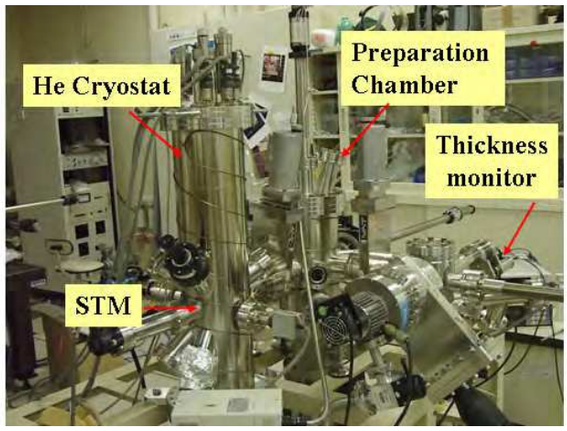

Fig. 5. UHV-LT-STM equipped with the facilities for sample preparation, sputtering and heating. Base pressure is ~~3× 10^{-9} Pa, the lowest temperature is ~8.7 K.

For the photon detection system in figure 4, STML experiments were performed with the conductive optical-fiber probes at RT and at about 80 K using liquid nitrogen. Photons induced by injecting electrons to the surface are collected into the STM probe and transferred to the outside photon detectors through several optical fiber connections. Several measurement modes of STML have been developed, i.e.: photon mapping, fixed-point optical spectroscopy, spectrum mapping spectroscopy (Nishitani et al., 1998), and spectroscopic imaging (Hoffmann et al., 2002). The latter two methods are only possible in very sensitive setups. In this study, two kinds of photon detection systems have been developed. One is the low-noise single photon counting system for quantitative photon mapping and the other is a fixed point optical spectroscopy. The single photon detection system is composed of a Peltier-cooled photomultiplier tube (PMT; Hamamatsu Photonics, R943-02), a discriminator, and a pulse counter. The PMT is set in the cooling system, which can not only cool it down to around -30°C but also acts as an effective electromagnetic

shield. The photons transferred through the optical fibers are focused on the center of the GaAs(Cs) photocathode surface using a condenser lens system. Although the PMT has a sufficiently high sensitivity over a wide spectral range from UV to NIR (160 to 930 nm), the effective cooling system can realize significantly low dark counts of ~3 counts/s (cps). A single TTL pulse is generated from a single voltage pulse caused by a single photon injection into the PMT. The pulse counter measures the number of the generated TTL pulses and outputs the analog voltage signal, which is proportional to the number of the pulses detected per a gate time. Connecting the analog output of the photon counter to the external input of the STM controller, simultaneous photon mapping with STM scanning is realized. Typical gate time for a photon mapping is 50 ms.

To perform STML spectroscopy, photons emitted from a fixed position are introduced to a multichannel spectrometer composed of an optical monochromator and a liquid-nitrogen cooled CCD detector. The monochromator is a Czerny-Turner type triple grating monochromator with a focal length of 300 mm (Acton Research Corp., SpectraPro-300i). The liquid nitrogen cooled CCD detector is operated at the fixed temperature of -110°C and has a back-illuminated CCD array with large pixels of 1,100×330 (Princeton Instruments, LN/CCD-1100PB). STM images presented here are all taken in topographic mode at a constant tunneling current. The tunnel bias is defined as the voltage applied to the sample. The practical set up of this photon detection system is shown in figure 6.

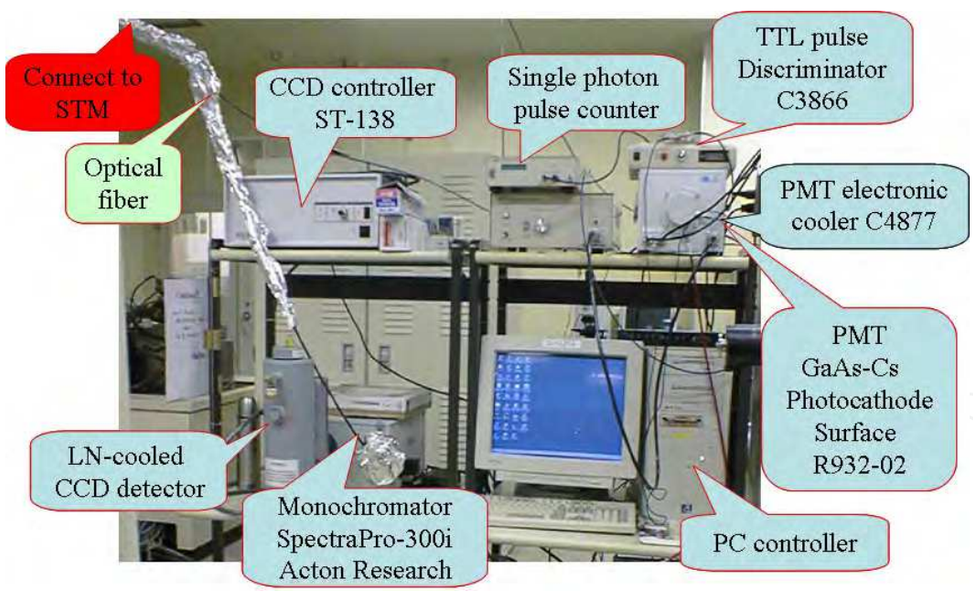

Fig. 6. Photon detection system for the measurements of STML.

2.3 Photon detection efficiency of STML

In order to perform a quantitative photon mapping of STML, light-detection efficiency of the photon detection system should be properly estimated. A schematic illustration of transmission and detection of STM-induced photons is shown in figure 7.

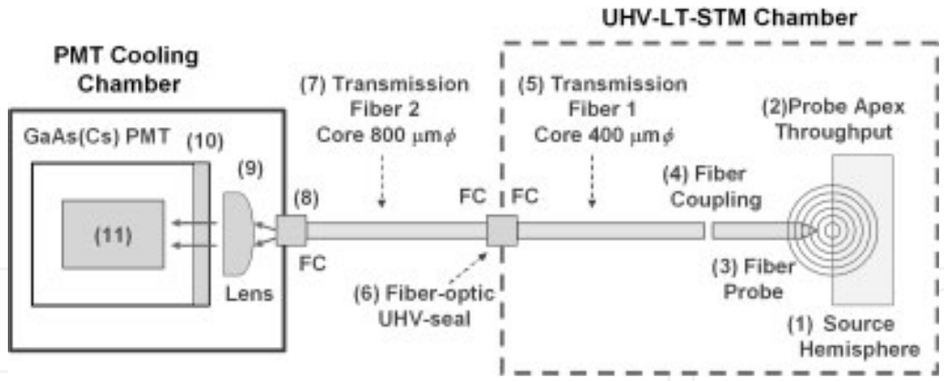

Fig. 7. Schematic illustration of transmission and detection of STML. From the photon source to the photocathode surface of the PMT, photons are transmitted through an optical fiber probe (core: 100 μmϕ), a first transmission fiber (core: 400 μmϕ), a fiber-optic UHV-seal with FC-type receptacles, a second transmission fiber (core: 800 μmϕ), a condenser lens with a FC-receptacle, and the PMT input window.

Firstly, the light source is located just under the probe apex. If the photons are uniformly emitted in space, approximately half of the photons can propagate to the vacuum-side hemisphere (1). Part of light escaped from the surface is collected into the probe with a specific throughput (2). From the probe apex to the photocathode surface (11) of the PMT, photons are transmitted through an optical fiber probe (3: numerical aperture, NA = 0.2, core 100 μmϕ), a fiber coupling (4), a first transmission quartz fiber (5: NA = 0.2, core: 400 μmϕ) in UHV, a fiber-optic UHV-seal with FC-type receptacles (6), a second quartz transmission fiber (7: Na = 0.2, core: 800 μmϕ), a FC-receptacle (8), a condenser lens to make a parallel light (9), and the PMT input window (10). Each optical path or connection has certain reflection and transmission losses. The total throughput of the light transferred from the tip apex to the photocathode of the PMT is approximately ~30% using the previously reported values by Murashita (1999). The quantum efficiency of the PMT (11) is 10–20% over a wide spectral range from UV to NIR (200 to 850 nm). The last task is to estimate collection yield of the fiber probe. In the case of an optical fiber with a flat surface, collection yield can be evaluated as follows. When light emitted from a point source is collected with an optical fiber located at optical far-field, the solid angle of collection is expressed by $2\pi(1-\cos(\sin^{-1}(NA)))$ if the fiber end is sufficiently close to the source (Arafune et al., 2001). Assuming NA = 0.2 for a quartz optical fiber, the solid angle of collection is 0.13 steradian, which corresponds to ~2 % of the hemisphere solid angle (2π). With fiber-probe collection, on the other hand, luminescence is collected at optical near-field into the apex of the probe located very close to the sample surface. Macroscopic shape of the probe apex is a cone, whose apex angle (2θ) is ~60° for our case, as shown in Figure 8(a). In this case, the collection solid-angle of the emitted photons can be evaluated by the cone solid angle $\Omega = 2\pi(1-\cos\theta)$. Since θ is ~30°, the collection solid angle is ~0.84 steradian, which corresponds to ~13% of 2π. In order to propagate within an optical fiber by total internal reflection, incident light should be injected within the limited acceptance cone. Although the gradually tapered shape can collimate the injected light into the acceptance cone with half angle θ_a = 11.5°, a fraction of the photons may propagate out of the fiber due to imperfect total internal reflection. From a microscopic point of view, the probe apex is not a real cone but has a rounded apex with a curvature of ~100 nm as shown in figure 8(b).

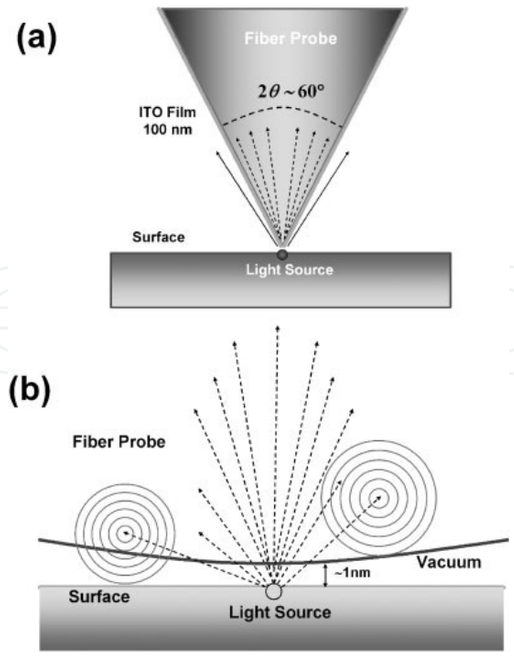

Fig. 8. (a): Schematic macroscopic representation of photon collection of STML with an ITO-coated optical fiber probe. The shape of the fiber probe can be approximated to a circular cone with half angle (θ) of around 30°. (b): Schematic microscopic illustration of near-field interaction between an optical fiber STM probe and a photon source at surface. Most of the emitted photons are injected into the fiber probe and some are transferred to propagating waves by scattering with nanometer-scale objects located in optical near-field.

Since the photons are generated in the nanometer-scale region at the surface and the distance between the probe and the surface is typically within one nanometer, most of the photons emitted to the vacuum are first captured into the probe apex within the optical near-field. As a result, enhanced collection yield of light into the fiber probe is expected due to the near-field detection (Murashita, 1999). Here we have assumed that the near-field enhancement can roughly compensate for the propagation loss caused by the imperfect total internal reflection. Taking into account the transmission efficiency of the ITO thin film (~75%), the collection yield of the optical fiber STM probe can be roughly estimated as ~10 %. Compared with reported throughput values (from ~10^{-5} to ~10^{-1}) of NSOM fiber probes with flat apertures (Ohtsu, 1998), the estimated collection yield of the fiber probe corresponds roughly to the best values of NSOM probes. Compared with the conventional far-field detection configurations, the collection yield ~10% of the fiber probe is as good as one of the best values (~9%) of the state-of-the-art lens detection system (Hoffmann et al., 2002). As will be shown later, the estimated collection yield of the fiber probe should be validated experimentally. By multiplying the above estimated values for the light collection efficiencies of the STM-luminescence detection system, total detection efficiency of the emitted photons (200–850 nm) is estimated to be ~0.15–0.3%.

2.4 Samples used for the measurement of STML

Samples prepared for the STML experiments were (1) a Zn-doped p-type GaAs (001) wafer with carrier concentration of ~1 × 10^{19} cm^{-3}, (2) a Si-doped n-type GaAs (001) wafer with

carrier concentration of ~1 × 10^{18} cm^{-3} , (3) an Au(111) film on freshly cleaved mica substrate. In order to produce a clean GaAs (110) surface, the samples were cleaved in ultrahigh vacuum in the sample preparation chamber. Immediately after the cleavage, the samples were transferred to the LT-STM chamber for the STML measurements. The Au(111) film with a thickness ~200 nm on freshly cleaved mica substrate is fabricated by the use of DC magnetron sputtering followed by an in-situ annealing at ~300 ◦C for 20 min. Cleaning of the Au(111) films were performed by a couple of cycles of Ar ion sputtering (~1 keV) and subsequent annealing at about ~600 K.

3. Results and discussions conclusion

3.1 High-resolution STM image using an ITO-coated fiber probe

Topographic STM images of a cleaved p-type GaAs(110) surface taken with a conventional tungsten tip at 100 K and with the optical fibre probe are compared in figure 9.

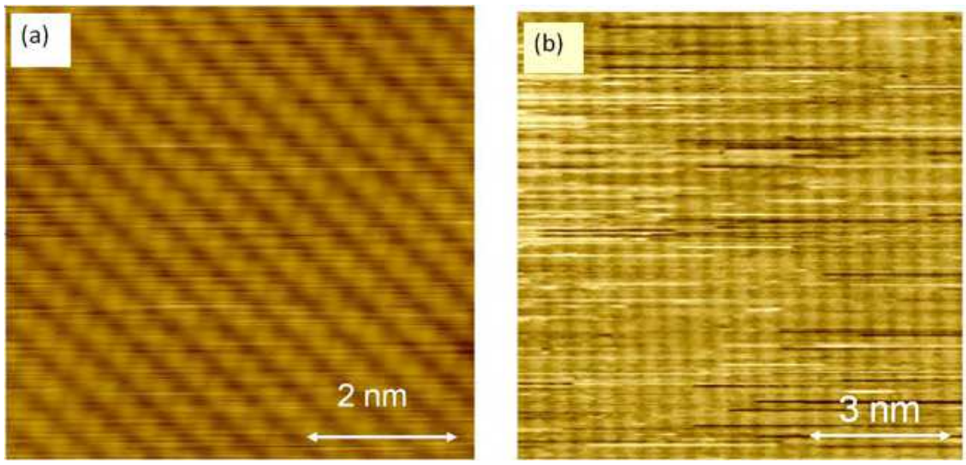

Fig. 9. STM topography images of cleaved GaAs(110) surfaces taken with (a) a W tip at RT (7.6×7.6 nm^2, -1.8 V, 0.2 nA); (b) an ITO-coated optical fiber probe at RT (10× 10 nm^2, -1.5 V, 0.2 nA).

Both images show the typical features of the relaxed GaAs(110) surface, where buckled dimer rows consisting of Ga atoms and As atoms are running along the ($\bar{1}$10) direction. The overall features of both images are consistent with the previously reported atomic-resolution STM images on GaAs(110) surfaces [Yokoyama & Takiguchi 2001; Ohtsu 1998]. The observed STM imaging quality using the optical fibre probe is a little bit worse than that with a conventional electrochemically sharpened tungsten tip [Ohtsu 1998].

3.2 STML from p-GaAs(110) surface using an ITO-coated fiber probe

3.2.1 The bias dependence of STML

Figures 10(a) and (b) show the bias dependencies of the STML intensity on the p-type GaAs(110) surface observed by the ITO-coated optical fiber probe at RT and 80 K, respectively.

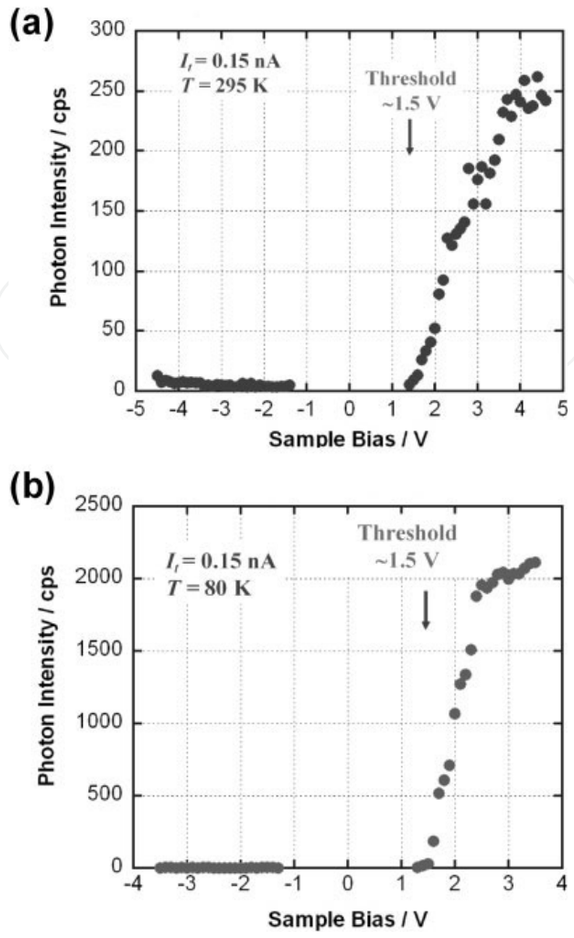

Fig. 10. Bias dependencies of STML intensity on a p-type GaAs(110) surface (Zn-doped) observed by an ITO-coated optical fiber probe at 295 K (a) and at 80 K (b). In both cases, threshold bias voltage of STML is at 1.5 V, which corresponds to a band-gap of GaAs. Photon intensity saturates around the sample bias voltage of ~3.5–5.0 V, where the quantum efficiencies at 295 and 80 K are 1.8 ×10^4 photons/electron and 1.5 ×10^3 photons/electron, respectively. Tunneling current I_t =0.15 nA.

The tunneling current was kept constant at 0.15 nA during the measurements by a feedback control. Much more intense STML has been observed for positive sample bias than for negative polarity. At the positive sample biases, threshold of STML is observable at ~1.5 V and saturates around the sample bias voltages of ~3 V. Typical maximum intensities of STML observed at 295 and 80 K are ~1.7× 10^3 and 1.4 ×10^4 cps/nA, respectively. The corresponding maximum quantum efficiencies (the number of emitted photons per an electron) at 295 and 80 K are ~1.8 ×10^4 and ~1.5 ×10^3 photons/electron, respectively. The quantum efficiency value (~1.8 ×10^4) at 295 K shows a good agreement with the previously reported value (~1 × 10^4 photons/electron) of STML from p-type GaAs regions of cleaved (110) GaAs/Al-GaAs heterostructures at RT (Abraham et al., 1990). Therefore, the total detection efficiency (about 0.15%) of the single photon counting system is estimated quite reasonably. In the positive polarity, the observed threshold voltage (~1.5 V) of STML corresponds closely to the direct band gap energies (1.424 and 1.493 eV) of GaAs at RT and

80 K (Madelung, 1996). In the case of p-doped semiconductors, the Fermi level is located around the top of the valence band and the major mechanism of the STML is radiative recombination of majority holes in the valence band and the injected electrons in the conduction band. To inject electrons into the conduction band, application of certain bias voltage is required, which almost corresponds to the band gap energy of GaAs in this case. On the contrary, in the negative polarity case, the STML intensity is much lower than the positive polarity case. The possible mechanism is direct recombination of electron-hole pairs created by the impact ionization of injected electrons.

3.2.2 The spectroscopy of STML

We performed spectroscopic studies not only at RT but also at low temperatures. Figure 11 is a comparison of the optical spectra of STML from a p-GaAs(110) surface obtained at three different temperatures (295, 85 and 18 K).

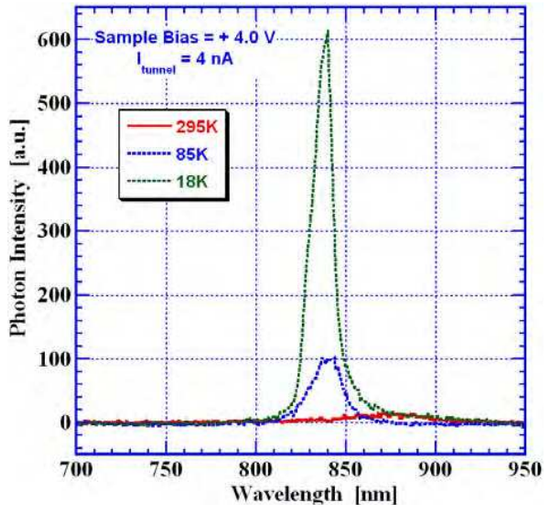

Fig. 11. A plot of near-field optical spectra of STML from a cleaved p-type GaAs(110) surface obtained with an ITO-coated optical fibre probe at 295, 85 and 18 K. The spectra were taken with a fixed sample bias (+4.0 V) andwith a constant tunnelling current of 4 nA.

The spectra were taken with positive sample bias (+4.0 V) and constant tunnelling current of 4 nA. Both a significant increase in the number of emitted photons and a sharpening of the peak shapes are observed with decreasing temperature. Also the peak position shift towards lower wavelength (blue shift) with decreasing temperature. The direct band gap of GaAs at 85 and 18 K can be empirically calculated as 1.507 eV (823 nm) and 1.518 eV (817 nm), respectively [Madelung,1996]. At sufficiently low temperatures, majority carriers (holes) are frozen on impurities [Yu & Cardona, 1996]. Taking into account the binding energy of a Zn acceptor (30.6 meV), the radiation energies of the exciton decay in GaAs at low temperatures can be estimated as 1.487 eV (834 nm) at 18 K and 1.476 eV (840 nm) at 85 K. The observed peak positions are 837 nm at 18 K and 840 nm at 85 K, which show good agreement with the estimated photon energies as above. Thus the dominant mechanism of STM-PEat lowtemperatures (T < 85 K) can be attributed to the radiative recombination of the injected free electrons with the majority holes trapped on the acceptors, which is known as a free-to-bound transition [Yu & Cardona, 1996].

3.2.3 The spatial distribution of STML

Spatial distribution of the STML can be visualized by multi-channel recording of STM-related data (topography, current, conductance, etc.) and photon intensity as a function of lateral position of the STM probe. Simultaneously obtained STM topography images and near-filed photon maps are obtained from the cleaved p-type GaAs(110) surface using the ITO coated probe. The experiment has been performed at 80 K keeping the tunneling current constant at 0.15 nA. At low temperatures, major photon emission process in p-GaAs can be attributed to the radiative recombination of injected electrons and major holes. By using this photon mapping technique, we have observed a significant decrease of STML intensity around the heavily-doped Zn accepter atoms located at the sub-surface regions of the GaAs(100) plane. Figures 12 (a) and (b) show an STM topography image and an STML map obtained simultaneously on the p-GaAs(110) surface. The protrusions appearing on the STM topography image correspond to the Zn dopants located at the sub-surface layers (de Raad et al., 2001; Zheng et al., 1994). The apparent height of the protrusions is related to the depth of the Zn dopants in the sub-surface layers.

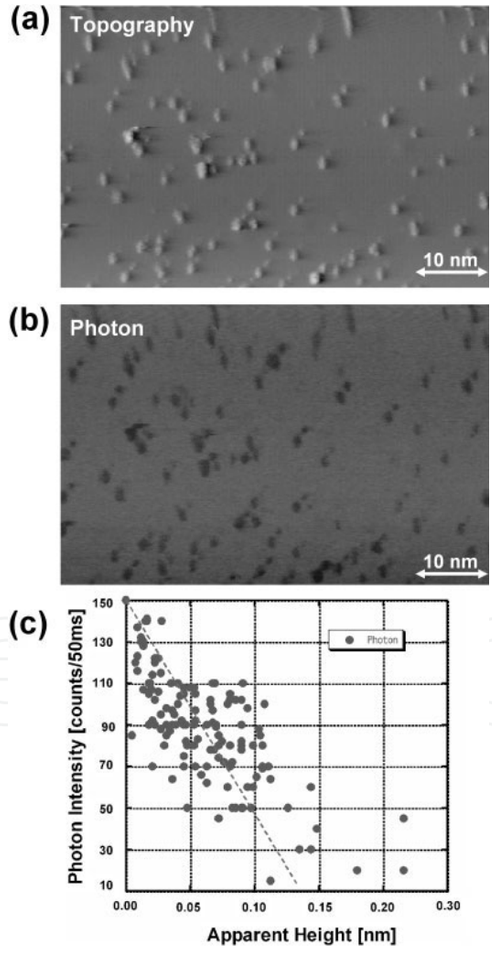

Fig. 12. Simultaneously obtained STM image (a) and a photon map (b) on a p-type GaAs(110) surface at 80 K using an ITO-coated optical fiber probe. (V_{sample} =+2.5 V, I_t =0.15 nA, scan size =59 ×39 nm). (c) : Relation between the apparent height and the STML intensity at the Zn dopant positions.

The protrusion with the highest apparent heights can be assigned to the Zn dopants in the first sub-surface layer. The protruding nature of the Zn dopants in the constant-current imaging is the result of enhanced tunneling near the core of Zn acceptor in GaAs (Zheng et al., 1994).
What is more interesting here is the spotty dark re- gions appearing on the near-field photon map in figure 12 (b). Those spots correspond to the locations of the Zn dopants. It should be noted that the individual dopants has been resolved by near-field STML photon mapping for the first time. Figure 12(c) shows the relation between the STM apparent heights and the STML intensities observed at the core positions of the Zn dopants. It is found that the STML intensity decreases significantly with the increase of the apparent height. Since the optical spectroscopy of the STML on the Zn dopants and on the normal terraces shows the same spectral features in shape and peak position, the basic luminescence mechanism itself should be the same, that is, the radiative recombination of the electron-hole pairs. Thus the decrease of the emitted photons can be attributed to the decrease of the number of injected electrons into the conduction band or to the decrease of the number of majority holes in the valence band.

3.2.4 The mechanism of STML

Figure 13 shows a schematic band diagram that illustrates the electron tunnelling process between the ITOcoated fibre probe and a p-GaAs(110) surface with positive sample bias. Since the sample is a heavily doped p-type GaAs(110), the Fermi level lies just above the valence band maximum (VBM). By applying a positive bias voltage *(Vs)* to the sample, the tunnelling electrons can get the injection energy of *eVs* measured from the VBM [Murashita & Tateno, 2001]. When the injection energy becomes larger than the direct band gap *(Eg)* of the sample *(eVs > Eg)*, it is possible to inject the tunneling electrons into the conduction band. At RT the injected electrons in the conduction band lose their energy through thermalization until they reach the conduction minimum (CBM). Then direct recombination process of the injected electrons and majority carriers (holes) causes the emission of photons.

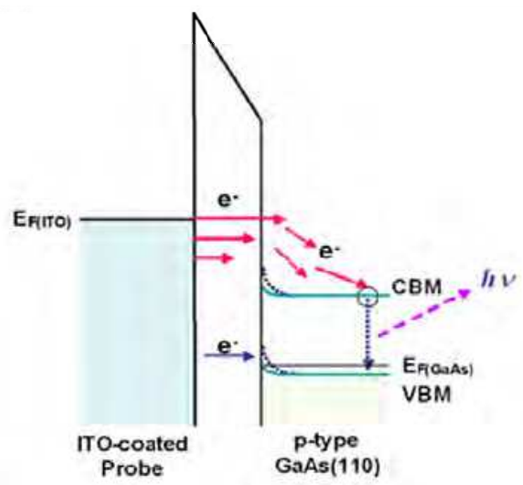

Fig. 13. A schematic energy band diagram illustrating the electron tunnelling process between the ITO-coated fibre probe and a p-type GaAs(110) surface with positive sample bias.

3.3 STML from n-GaAs(110) surface using an ITO-coated fiber probe

3.3.1 The bias dependence of STML

Figures 14 (a) and (b) show the tunnel-bias dependence of the STMEL intensities from the surface of n-type GaAs(110) induced by the ITO-coated optical fibre probe at RT and 80 K, respectively.

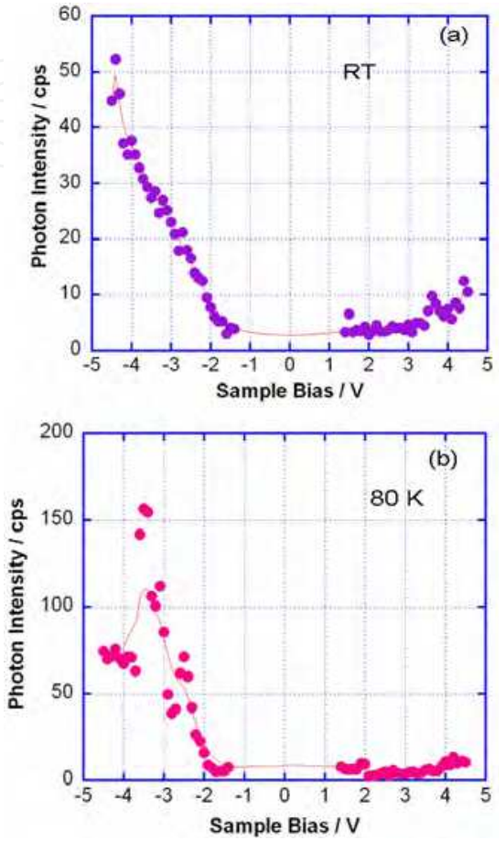

Fig. 14. Bias dependence of STML intensities from surface of n-type GaAs(110) at RT (a) and 80 K (b). At both temperatures, the STML becomes observable when the applied sample bias exceeds −1.5 V and shows higher intensity at negative bias than that at positive bias (tunnelling current = 0.15 nA). The dotted lines are drawn by a polynomial fit to the experimental data, which shows the continuous changes in the STML intensities versus bias.

The tunnelling current is kept at 0.15 nA by a feedback control. At both temperatures, the STML becomes observable when the applied sample bias exceeds −1.5 V in the negative bias region, and saturates around a sample bias of −5.0 to −6.0 V. The direct band gaps of GaAs at RT and 80 K can be calculated empirically as 1.424 and 1.507 eV, respectively [Evoy et al,1999; Alvarado et al, 1991;Rossi et al, 1970], which are in good agreement with the above observed threshold 'turn on' voltage (−1.5 V) shown in figures 14(a) and (b). In the positive bias region, a weak photon emission can be observed when the bias exceeds~+3.5 V. At RT the maximum value of the STML intensity at negative sample bias is about five times higher than that at positive sample bias, as shown in figure 14(a), while at 80 K the maximum value of STML intensity at negative sample bias is about 15 times higher than that at positive sample bias, as shown in figure 14(b). This can be explained by the different recombination

process of hole– electron pairs, which will be discussed below, along with the optical spectroscopy data. The large difference in photon emission intensity at RT and 80 K can probably be attributed to the fact that majority carriers (electrons) are frozen on impurities at sufficiently low temperatures [Yu & Cardona,1996], which leads to the increase in radiation efficiency of the exciton decay in GaAs. The maximum quantum efficiency (the number of emitted photons per electron or hole) at RT and 80 K can be calculated as ~3×10^{-5} and ~1×10^{-4} (photons/electron), respectively.

3.3.2 The mechanism of STML

Figure 15 is a schematic energy band diagram illustrating the STML process on the surface of n-type GaAs(110) at both polarities.

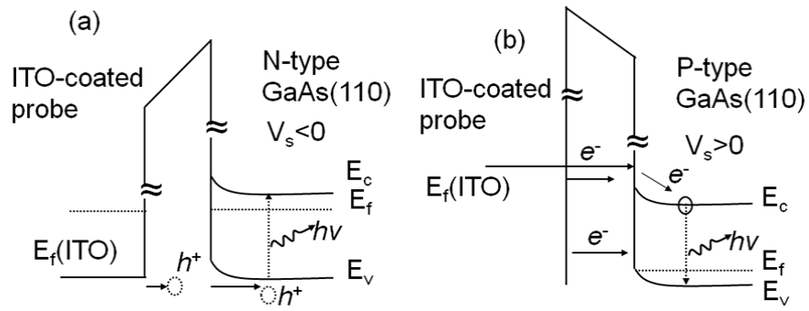

Fig. 15. Schematic energy band diagrams illustrating STML process on the surface of n type GaAs(110), showing two kinds of radiative recombination process of bulk hole–electron pairs: (a) direct recombination of injected holes from the tip with majority carriers (electrons) into n-type GaAs at negative sample bias, and (b) recombination of extra bulk hole–electron pairs created by an impact ionization effect of energetic electrons injected from the tip into the surface of n-type GaAs at positive sample bias.

In figure 15(a), at a sufficient negative sample bias, the tip Fermi level is aligned with the valence band, and holes are injected from the tip side into n-type GaAs (electrons are tunnelled out). Injected at low biases (<−1.5 V in this experiment), carriers are trapped at the surface. Injected at higher biases (>−1.5 V), carriers may reach the bulk and recombine radiatively with readily available majority carriers, emitting light of an energy equal to the bulk band gap energy, $Eg = h\nu$. The STML generated at positive sample bias rarely occurs for n-type semiconductors at positive sample bias. The most likely reason is probably due to an impact-ionization effect, which is shown in figure 15(b). In figure 15(b), under a sufficient positive sample bias (~+3.5 V in this experiment), the electrons injected from the tip side into the conduction band can cause an impact ionization effect that creates extra holes. The radiative recombination of the extra holes with the majority carriers (electrons) generates a relatively weak STML due to its large threshold voltage (~+3.5 V) in generating extra bulk hole–electron pairs. Both above cases will generate carriers which ultimately recombine over the band gap and thus yield a peak at ~1.5 eV.

3.4 Development of Au/ITO dual-layer-coated optical fiber probe

In the case of HET-type STM-luminescence such as the case of p-GaAs, the electronic property of the tip materials does not significantly affect the luminescence efficiency. However, in the case of TIP-type STM-luminescence, proper selection of the tip material is

very important to enhance the quantum efficiency since the electronic properties of both tip and surface contribute the TIP-type STM-luminescence (Johansson, 1998; Johansson et al., 1990). Furthermore, the near-field photon detection using an ITO-coated fiber probe has a higher and more stable photon detection efficiency of STML than that of far-field photon detection. However, the electron injection efficiency, STM image resolution and tunneling stability of the semiconductor ITO-coated fiber probe are generally lower than those of metal tip. Because the ITO layers for the commercially available ITO-coated fiber probes are normally very crystalline or smoothly coated on the fiber probe with a symmetrical geometry and sharp tip apex, they can easily crash with low durability and change the tunneling condition during scanning process. Therefore, it is necessary to coat a thin metal layer such as Au, Ag to improve the performance of ITO-coated fiber probe. In this research, the thin Au/ITO dual layer is deposited by DC magnetron sputtering on the surface of the tip apex of the ITO-coated fiber probe to improve its tip geometry, imaging quality and electron injection efficiency. Sputtering of the ITO layer was performed using a ceramic high-density ITO target (5 wt% SnO_2) at ~1×10^{-1} Pa in a pure Ar/O_2 gas mixture with the distance between the target and tip holder fixed at 10 cm. The DC power was maintained at 100 W for all the deposition. The base pressure of the chamber was ~1×10^{-4} Pa. Sputtering of the Au layer was performed using an Au metal target (purity: 99.95%) in a pure Ar gas (~1×10^{-1} Pa) environment after depositing the ITO layer.

Figure 16(a) shows a SEM image of the fabricated Au/ITO dual-layer-coated fiber probe. The deposited Au/ITO dual layer around the tip apex looks smooth and the coated tip apex looks transparent by naked eye. The outer Au layer is confirmed by the corresponding AES Au map and spectrum analysis, as shown in figures 16(b) and (c), respectively. The Au map in figure 16(b) matches very well with the SEM image in figure 16(a) and shows that the Au layer uniformly covers the tip apex. The Au NOO, M_5NN, M_4NN peaks in figure 16(c) appeared constantly when randomly examined at points around the tip apex region; this also indicates the uniform coverage of the Au layer.

The thickness of the Au layer is a critical parameter to obtaining a better yield of high electron injection efficiency and near-field photon detection efficiency. We measured the optical transmission with UV-2450 spectrophotometers, Shimadzu, Japan and the electric resistivity by the four-probe method for Au films of various thickness, uniformly deposited on a glass substrate by sputtering, to determine the appropriate thickness of the Au layer to realize a better combination of conductivity and transparency. The measured electric resistivity and optical transmission values versus film thickness are shown in figures 17(a) and (b), respectively.

Figure 17(a) illustrates a spread of conductivity at low thickness values (<25 nm). This is because the resistivity of metal deposits at low thickness is complicated by the dynamics of film nanostructure [Lidzey et al, 1997]. The electric resistivity of the Au films is almost constant with variation of film thickness up to 1000 nm, whereas the optical transmission decreases monotonously with the film thickness. The appropriate thickness value of the Au film is determined as 13 nm, where both a resistivity ~1.5×10^{-5} Ωcm and a high optical transmission ~48% are achieved. This conductive value is enough for tunneling and getting a better yield of high electron injection efficiency in the STM tunneling junction. Based on the above results, the optical collection efficiency of the fabricated Au/ITO dual-layer-coated fiber probe is estimated as ~10%, which is similar to that of the standard optical tip [Tsuruoka et al, 1998].

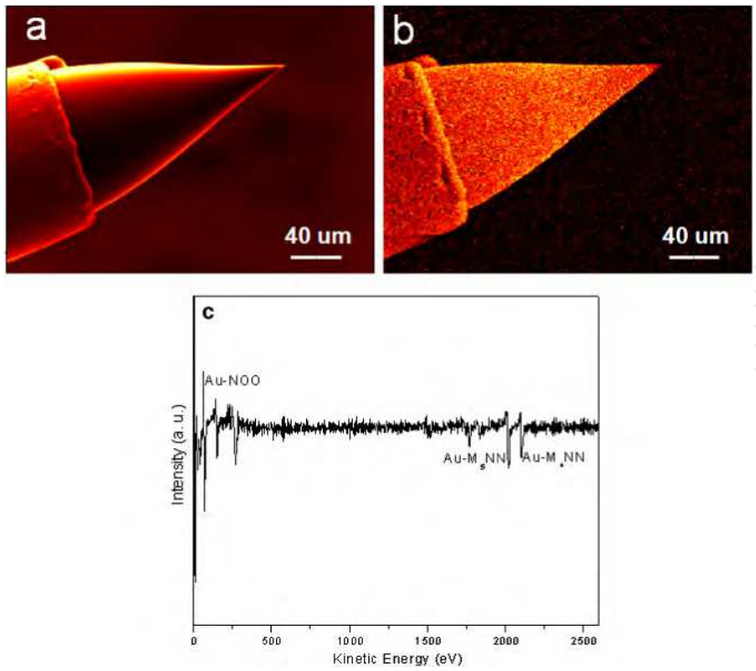

Fig. 16. (a) SEM image of the fabricated Au/ITO-coated fiber probe; (b) corresponding Au Auger map which shows a uniform coverage of the Au layer around the tip apex; (c) typical AES spectrum randomly examined at the points around the tip apex region.

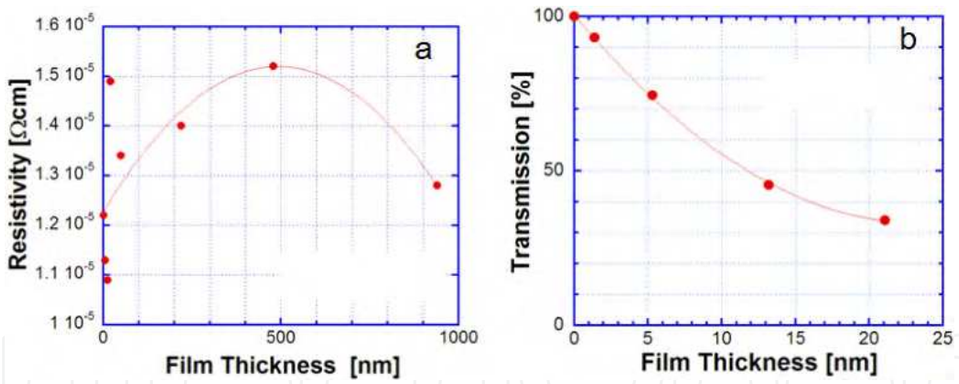

Fig. 17. (a) Resistivity versus Au film thickness measured by the four-probe technique; (b) optical transmission versus Au film thickness. A best combination point of resistivity with transmission is determined at ~13 nm in thickness.

High-quality STM imaging with a herringbone reconstruction on a Au(111) surface on mica is clearly observed by using this Au(13 nm)/ITO(50 nm) dual-layer-coated fiber probe, as shown in figure 18.

On the contrary, the herringbone reconstruction is difficult to observe using the pristine ITO-coated fiber prober without the Au/ITO dual coating layer.

For comparison, the STML is investigated on the surface of Au(111)/mica using both the Au/ITO dual-layer-coated fiber probe and the pristine ITO-coated fiber probe at RT. Figures 19(a) and (b) are the measured photon intensity versus the sample bias on Au(111)/mica by use of these two kinds of fiber probes, respectively.

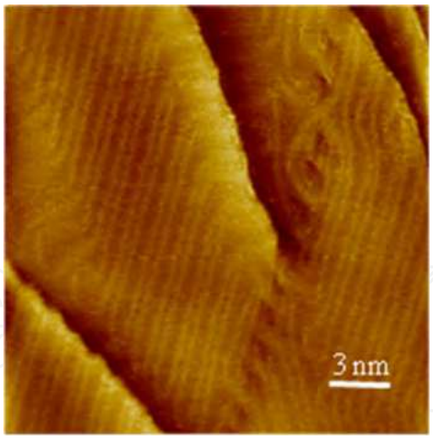

Fig. 18. STM image of a Au(111) surface using the Au (13 nm in thickness)/ITO-coated fiber probe, which shows a clear herringbone reconstruction structure. (Sample bias = −1.7 V, tunneling current = 0.15 nA, 20 nm × 20 nm).

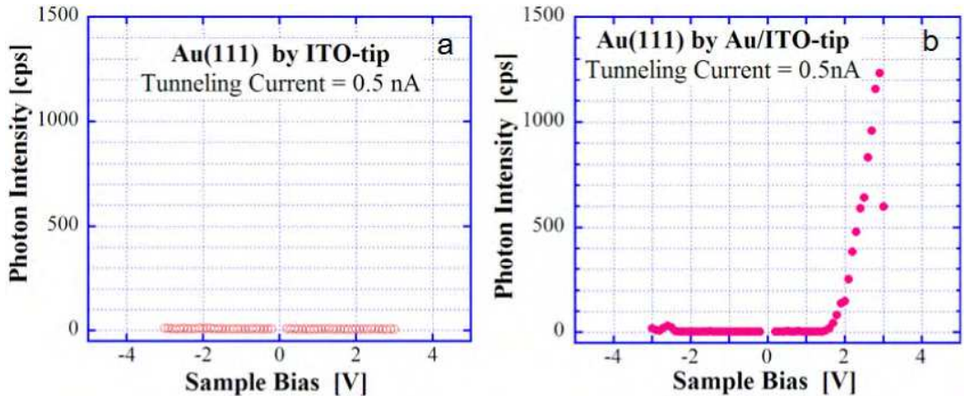

Fig. 19. Bias dependence of STML intensity from the Au(111) surface at RT (tunneling current = 0.5 nA): (a) using the ITO-coated fiber probe; (b) using the Au/ITO-coated fiber probe. The STML is generated only in the case of (b), with a maximum quantum efficiency ~7 × 10−4 photon/electron at a sample bias of +3 V, whereas the STML is too weak to be observed in case (a).

The surface plasmon-mediated emission is hard to generate without Au coating (see figure 19(a)) whereas the maximum quantum efficiency of ~7 × 10^{-4} photons per electron was obtained at a sample bias of ~2.5 V using the Au/ITO dual-layer-coated fiber probe. The Au layer shows an effective enhancement of the intensity of Plasmon mediated STML from the surface of Au(111)/mica at positive sample bias. Because the plasmon-mediated STML is generated by inelastic tunneling [Hoshino & Yamamoto 2003], it is reasonable to believe that such a kind of enhancement is attributed to the improvement of the outside Au layer on the sharpness and electron injection efficiency of the ITO-coated fiber probe. It is worth noting that the plasmon-mediated STML at negative sample bias is usually very weak (as can be seen from the weak emission peak at ~−2.8 V in figure 19(b)) compared to that at positive sample bias. The main reason is probably attributed to the symmetry of the tip apex and the difference of crystallinity between the Au layer on the surface of the fiber probe and the Au(111) on mica substrate.

4. Conclusion

An ultrahigh-vacuum low-temperature scanning tunneling microscope with a conductive and optically transparent probe was employed to perform detailed analyses of STML from a cleaved Zn-doped p-type GaAs(110) surface and Si-doped n-type GaAs(110), respectively. Photons generated in a nanometre-scale area just under the STM probe can be collected effectively within the optical near-field region through the apex of the optical fibre tip. We observed a strong photon emission at positive sample biases where electrons are injected into the p-GaAs(110) surface. While under both bias polarities, we observed nanoscale STML from the surface of n-type GaAs(110) at RT and 80 K. The developed Au/ITO dual-layer-coated optical fiber probe for STML exhibits high performance in further improving the quality, stability and reproducibility of STM imaging and STML, and enhancing the electron injection efficiency from the tip apex to generate high-intensity plasmon-mediated STML. This novel conductive and transparent optical fiber probe provides an effective way to construct a multifunctional STM and for the fabrication of highly efficient nanoscale light sources.

5. Acknowledgment

We would like to thank for the help of Ms. N. Niori in the experiment work, and the supports from National Natural Science Foundation of China (21173041 from National Natural Science Foundation of China (21173041), National Basic Research Program of China (973 plan, 2012CB619401), Open project of Jiangsu Key Laboratory for design and Manufacture of Micro-Nano Biomedical Instruments, China(JSNBI201101) and Pairs of Talent Foundation of Jiangsu, China in writing this chapter.

6. References

Abraham DL, Veider A, Scho¨nenberger Ch, Meier HP, Arent DJ, Alvarado SF. (1990). Luminescence in scanning tunneling microscopy on III-V nanostructures. *Appl Phys Lett* No. 56, pp.(1564–1566)

Arafune R, Sakamoto K, Meguro K, Satoh M, Arai A, Ushioda S. (2001). Multiple-fiber collection system for scanning tunneling microscope light emission spectroscopy. *Jpn J Appl Phys* No. 40, pp.(5450–5453)

Alvarado S F, Renaud P, Abraham D L, Schonenberger C, Arent D J, Meier H P. (1991). *J. Vac. Sci. Technol.* B No.9, pp.(409-413)

Binning G, H. Rohrer, Ch. Gerber, E. Weibel. (1982). *Physics. Rev. Lett*. No. 49, pp.(57-60)

Binning G, H. Rohrer, Ch. Gerber, E. Weibel. (1983). *Physics. Rev. Lett*. No. 50, pp.(120-123)

Binning G, C. F. Quate, Ch. Gerber. (1986). *Physics. Rev. Lett.* No. 56, pp.(930-933)

Berndt R, (1998). Scanning probe microscopy and spectroscopy. New York: Springer. pp. (97–134)

Berndt R, Gimzewski JK, Johansson P. (1993a). Electromagnetic-interactions of metallic objects in nanometer proximity. *Phys Rev Lett* No. 71, pp.(3493–3496).

Berndt R, Gaisch R, Schneider WD, Gimzewski JK, Reihl B, Schlittler RR, Tschudy M. (1995). Atomic-resolution in photon-emission induced by a scanning tunneling microprobe. *Phys Rev Lett* No. 74, pp.(102–105)

Berndt R, Gimzewski JK. (1993). Photon emission in scanning tunneling microscopy: Interpretation of photon maps of metallic systems. *Phys Rev B* No. 48, pp.(4746–4754)

Berndt R, Gaisch R, Schneider WD, Gimzewski JK, Reihl B, Schlittler RR, Tschudy M. (1993b). Photon-emission from adsorbed C_{60} molecules with subnanometer lateral resolution. *Appl Phys A* No.57, pp.(513–516)

Daisuke Fujita, Keiko Onishi and Noriko Niori. (2004). Light emission induced bytunnelling electrons from a p-type GaAs(110) surface observed at near-field by a conductive optical fibre probe, *Nanotechnology* No. 15 , pp.(S355-S361)

de Raad G J, Bruls D M, Koenraad P M, Wolter J H. (2001). *Phys. Rev.* B, No. 64, pp.(075314–075320)

Dos Sandos DA, Bredas JL, Logdlund M, Salaneck WR. (1999). Electroluminescence in conjugated polymers. *Nature* No. 397, pp(121–128)

Downes A, Welland ME. (1998). Photon emission from Si(111)-(7x7) induced by scanning tunneling microscopy: atomic scale and material contrast. *Phys Rev Lett* No.81, pp.(1857–1860)

Downes A, Taylor ME, Welland ME. (1998). Two-sphere model of photon emission from the scanning tunneling microscope. *Phys Rev B* No. 57, pp.(6706–6714)

Dong Z. C, Guo X. L, A. S. Trifonov, P. Dorozhkin, K. Miki, K. Kimura, S. Yokoyama, S. Mashiko. (2004). Vibrationally Resolved Fluorescence from Organic Molecules near Metal Surfaces Induced by a Scanning Tunneling Microscope. *Phys. Rev. Lett.*, No.92, pp. (0868011-0868014)

Dong Z-C, Kar A, Zou Z-Q, Ohgi T, Dorozhkin P, Fujita D, Yokoyama S, Terui T, Yamada T, Kamikado T, Zhou M, Mashiko S, Okamoto T. (2002). Light emission from porphyrin molecules induced by a scanning tunneling microscope. *Jpn J Appl Phys* No. 41, pp.(4898–4902)

Evoy S, Harnett CK, Craighead HG, Keller S, Mishra UK, DenBaars SP. (1999). Low-temperature scanning tunneling microscope-induced luminescence of an InGaN/GaN multiquantum well. *Appl Phys Lett* No. 74, pp.(1457–1459)

Evoy S, Craighead H G, Keller S, Mishra U K , DenBaars S P. (1999). *J. Vac. Sci. Technol.* B No. 17, pp.(29-33)

Fujita D, Ohgi T, Deng W, Ishige K, Okamoto T, Yokoyama S, Kamikado T, Mashiko S. (2001). Photon emission induced by tunneling electrons from a Cu(100) surface covered with porphyrin molecules. *Surf Sci* No.493, pp.(702–707)

Friend RH, Gymer RW, Holmes AB, Burroughes JH, Marks RN, Taliani C, Bradley DDC, Garcia-Parajo M, Cambril E, Chen Y. (1994). Simultaneous scanning tunneling microscope and collection mode scanning near-field optical microscope using gold coated optical fiber. *Appl Phys Lett* No.65, pp.(1498–1500)

Guo X. L, D. Fujita, N. Niori, K. Sagisaka, and K. Onishi. (2007). Nanoscal electroluminescence from n-type GaAs(110) in tunnel junction, *Nanotechnology* No.18, pp.(195201-195204)

Guo X. L, Dong Z. C, A. S. Trifonov, S. Mashiko, T. Okamoto. (2003). Tunneling-induced molecular luminescence from nanoscale organic molecular layers on metal substrate *Appl. Phys. Lett.*, No.84, pp. (969-972)

Guo X. L, Dong Z. C, A. S. Trifonov, S. Mashiko, T. Okamoto. (2003). Role of molecules in tunneling current induced photon emission from the surface of a perinone

derivative molecular monolayer on Au(100) , *Phys. Rev. B*. No. 68, pp.(113403-113405)

Guo X. L, Dong Z. C., A. S. Trifonov, K. Miki, Wakayama, D. Fujita, K. Kimura, S. Yokoyama, S. Mashiko. (2004). Nanoscale organic electroluminescence from tunnel junctions, *Phys. Rev. B*, No. 70, pp. (233204-233207)

Guo X. L, Fujita D, Niori N, Sagisaka K and Onishi N. (2007). Scanning tunneling Microscopy luminescence from nanoscale surface of GaAs(110), *Surf. Sci.* No.601, pp. (5280-5284)

Hoffmann G, Kliewer J, Berndt R. (2001). Luminescence from metallic wells in a scanning tunneling microscope. *Phys Rev Lett* No.87, pp.(176803–176806)

Hoffmann G, Kro¨ger J, Berndt R. (2002). Color imaging with a low temperature scanning tunneling microscope. *Rev Sci Instrum* No. 73, pp.(305–309)

Hoshino M and Yamamoto N. (2003). *Mater. Res. Soc. Symp. Proc.* No.738, pp.(149-153)

Johansson P. (1998). Light emission from a scanning tunneling microscope: Fully retarded calculation. *Phys Rev B* No.58, pp.(10823–10834)

Johansson P, Monreal R, Apell P. (1990). Theory for light-emission from a scanning tunneling microscope. *Phys Rev B* No. 42, pp.(9210–9213)

Lidzey DG, Alvarado SF, Seidler PF, Bleyer A, Bradley DDC. 1997. Electroluminescence from a soluble poly(p-phenylenevinylene) derivative generated using a scanning tunneling microscope. *Appl Phys Lett* No.71, pp.(2008–2010)

Lidzey DG, Bradley DDC, Skolnick MS, Virgili T, Walker S, Whittaker DM. 1998. Strong exciton-photon coupling in an organic semiconductor microcavity. *Nature* No. 395, pp.(53–55)

Madelung O. (1996). Semiconductors: basic data. Berlin: Springer. p.101.

Murashita T. (1999). Optical system for tunneling-electron luminescence spectro/ microscopes with conductive-transparent tips in ultrahigh vacuums. *J Vac Sci Technol B* No.17, pp.(22–28)

Murashita T, Tateno K. (2001). Direct measurement of sub-10 nm-level lateral distribution in tunneling-electron luminescence intensity on a cross-sectional 50-nm-thick AlAs layer by using a conductive transparent tip. *Appl Phys Lett* No.78, pp.(3995–3997)

Murashita T, Tateno K. (2001). *Appl. Phys. Lett.* No. 78, pp.(3995–4002)

Nishitani R, Umeno T, Kasuya A. (1998). A study of metal films using a spectrally resolved photon map obtained by spectrum mapping measurements of STM-induced light. *Appl Phys A* No.66, pp.(S139–S143)

Ohtsu M. 1998. Near-field nano/atom optics and technology. Tokyo: Springer. p 71.

Rossi J A, Wolfe C M , Dimmock J O. (1970). *Phys. Rev. Lett.* No.25, pp.(1614-1618)

Sasaki S, Murashita T. (1999). Crossover energy where cathodoluminescence becomes comparable to electroluminescence in p-type GaAs observed by injecting tunneling electrons. *Jpn J Appl Phys* No. 38, pp.(L4–L6)

Sergei Kalinin, Alexei Gruverman, (2007). Scanning Probe Microscopy, Volume I, Springer,ISBN-10 : 0-387-28667-5, Springer Science+ Business Media, LLC, 233 Spring Street, New York, NY 10013, USA

Suzuki Y, Minoda H, Yamamoto N. (1999). STM light emission from Ag/Si(111). *Surf Sci* No. 438, pp.(297–304)

Thirstrup C, Sakurai M, Stokbro K, Aono M. (1999). Visible light emission from atomic scale patterns fabricated by the scanning tunneling microscope. *Phys Rev Lett* No. 82, pp.(1241–1244)

Tsuruoka T, Ohizumi Y, Ushioda S. (2003). Light intensity imaging of single InAs quantum dots using scanning tunneling microscope. *Appl Phys Lett* No.82, pp.(3257–3259

Tsuruoka T, Ohizumi Y, Ushioda S, Ohno U and Ohno H. (1998). *Appl. Phys. Lett.* No.73, pp.(1544-1547)

Uehara Y, Fujita T, Ushioda S. (1999). Scanning tunneling microscope light emission spectra of Au(110)-(2 ×1) with atomic spatial resolution. *Phys Rev Lett* No. 83, pp.(2445–2448).

Yokoyama T, Takiguchi Y. (2001). *Surf. Sci.* No. 482–485, pp.(1163–1168)

Yu P Y and CardonaM. (1996). *Fundamentals of Semiconductors* (Berlin: Springer) p 339

Zheng ZF, Salmeron MB, Weber ER. (1994). Empty state and filled state image of ZnGa acceptor in GaAs studied by scanning-tunneling- microscopy. *Appl Phys Lett* No.64, pp.(1836–1838)

IntechOpen

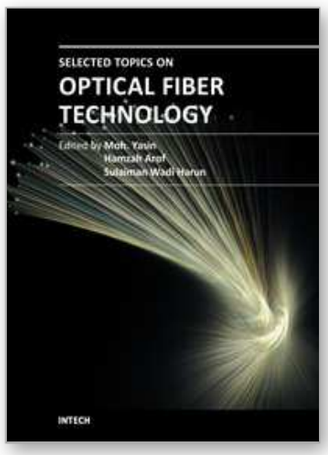

Selected Topics on Optical Fiber Technology

Edited by Dr Moh. Yasin

ISBN 978-953-51-0091-1

Hard cover, 668 pages

Publisher InTech

Published online 22, February, 2012

Published in print edition February, 2012

This book presents a comprehensive account of the recent advances and research in optical fiber technology. It covers a broad spectrum of topics in special areas of optical fiber technology. The book highlights the development of fiber lasers, optical fiber applications in medical, imaging, spectroscopy and measurement, new optical fibers and sensors. This is an essential reference for researchers working in optical fiber researches and for industrial users who need to be aware of current developments in fiber lasers, sensors and other optical fiber applications.

How to reference

In order to correctly reference this scholarly work, feel free to copy and paste the following:

Guo Xinli and Fujita Daisuki (2012). Novel Conductive and Transparent Optical Fiber Probe for Multifunctional Scanning Tunneling Microscopy, Selected Topics on Optical Fiber Technology, Dr Moh. Yasin (Ed.), ISBN: 978-953-51-0091-1, InTech, Available from: http://www.intechopen.com/books/selected-topics-on-optical-fiber-technology/multifunctional-fiber-

INTECH
open science | open minds

InTech Europe

University Campus STeP Ri
Slavka Krautzeka 83/A
51000 Rijeka, Croatia
Phone: +385 (51) 770 447
Fax: +385 (51) 686 166
www.intechopen.com

InTech China

Unit 405, Office Block, Hotel Equatorial Shanghai
No.65, Yan An Road (West), Shanghai, 200040, China
中国上海市延安西路65号上海国际贵都大饭店办公楼405单元
Phone: +86-21-62489820
Fax: +86-21-62489821

© 2012 The Author(s). Licensee IntechOpen. This is an open access article distributed under the terms of the Creative Commons Attribution 3.0 License, which permits unrestricted use, distribution, and reproduction in any medium, provided the original work is properly cited.

IntechOpen

IntechOpen